CrossMark
click for updates

CFD simulations on the effect of catalysts on the hydrodeoxygenation of bio-oil

Anjani R. K. Gollakota,[a] Malladi D. Subramanyam,[a] Nanda Kishore*[a] and Sai Gu*[b]

Bio-oil derived from lignocellulose biomass is an emerging alternative resource to conventional fossil fuel. However, the as-obtained unprocessed bio oil is oxy-rich, has low pH and contains high moisture, which suppresses the heating value; thus, its mixing with conventional fuel is not compatible. Therefore, studies on the upgradation of bio oil using catalytic hydrodeoxygenation (HDO) have become prominent in recent years. This study presents computational fluid dynamics (CFD) based simulation results on the effect of catalysts (Pt/Al_2O_3, $Ni-Mo/Al_2O_3$, $Co-Mo/Al_2O_3$) on the upgradation of bio oil using a hydrodeoxygenation process in an ebullated bed reactor. These numerical simulations are performed using an Eulerian multiphase flow module that is available in a commercial CFD based solver, ANSYS Fluent 14.5. Prior to obtaining the new results, the present numerical solution methodology is validated by reproducing some of the experimental results on the upgradation of bio oil available in the literature. Furthermore, the influence of weight hourly space velocities (WHSVs), operating temperature, and pressure inside the reactor for the different catalysts on the performance of HDO for bio oil upgradation in an ebullated bed reactor are delineated. It is observed that the gaseous stream products are higher in the presence of Pt/Al_2O_3 catalyst; phenols are higher when $Ni-Mo/Al_2O_3$ is used, and higher aromatics are obtained with the $Co-Mo/Al_2O_3$ catalyst. Finally, a comparison among the mass fraction of the individual species of three phases with respect to different catalysts for various combinations of WHSV, temperature and pressure values are presented.

Introduction

Demand for energy is increasing globally and is expected to double in coming years due to population growth and various developments in society. The major source of energy generation to meet the present necessities is from fossil fuels. This energy generation, which results in the emission of CO_2, leads to problems related to climate change such as global warming. Thus, it is a global challenge to counterbalance the environmental protection and generation of alternative sources of fuel to satisfy the demand. To address these challenges, mankind is stimulated to use renewable energies such as wind, solar, biomass and hydroelectricity, among which biofuels are emerging as a promising solution and alternative source of energy due to their sustainability and CO_2 neutral resources. These bio fuels are derived from the biological carbon fixation and mainly result from biomass feed stocks. Some interesting facts about biomass feed stocks are that they are free from sulphur, nitrogen and ash; thus, the emissions are also free from SO_x, NO_x, and CO_2. Because of their diversity, bio-fuels are

classified into various sections and named as renewable advanced bio fuels or next generation sustainable fuels. This classification is majorly dependant on the type of feedstock, conversion technology, product formed and carbon source. Bioethanol and bio-diesel are first generation biofuels derived from biomass, whereas second generation biofuels are derived from lignocellulosic biomass. However, the major obstacle for these biofuels is the degradation of the biomass. Therefore, third generation biofuels are derived from microalgae and cyanobacteria. The bio oil that is obtained from the pyrolysis of lignocellulosic biomass is unstable and has a high water content, low pH, high viscosity, low heating value, and is highly corrosive. According to Oasmaa et al.,[1] the produced bio-oil made of 300 different organic compounds mostly consists of (20–30 wt%) water, (15–30 wt%) lignin fragments, (10–20 wt%) aldehydes, (10–15 wt%) carboxylic acids, (5–10 wt%) carbohydrates, (2–5 wt%) phenols, (1–4 wt%) furfurals, (2–5 wt%) alcohols and (1–5 wt%) ketones. To overcome the deleterious properties of biomass pyrolysis oil, an upgrading process is required before its application. Currently, there are various techniques available to upgrade bio-oils into transportation fuels. They are catalytic hydrodeoxygenation (Furimsky[2]), zeolite upgrading (Adjaye and Bakhshi[3]), catalytic cracking (Hew et al.[4]), super critical technology (Tang et al.,[5] Zhang et al.[6]) and emulsification (Bridgwater[7]).

[a]*Department of Chemical Engineering, Indian Institute of Technology Guwahati, Assam – 781039, India. E-mail: nkishore@iitg.ernet.in*

[b]*Centre for Biofuel, School of Energy, Environmental and Agrifood, Cranfield University, UK. E-mail: s.gu@cranfield.ac.uk*

Research activities on the upgradation of bio-oils using HDO started in the 1970's. The first review on the accomplishment of the upgradation process of bio-oil through HDO was successfully explained by Furimsky.[2] Other pioneering work of Furimsky[8] explained the chemistry, difficulties in determining rate constants, problems associated with the presence of oxygen, the growing concerns of upgrading coal and biomass derived fuels in detail. This led to a paradigm shift in research towards techniques pertaining to upgrading bio-oils. Oyama[9] reported that the HDO process is similar to hydrodenitrogenation (HDN) but 10 times efficient than the later technique over vanadium nitride catalysts. Maggi and Delmon[10] published a review, and discussed various aspects related to the catalytic chemistry, kinetics, and mechanisms of HDO reactions using various model oxygenated compounds inline with the review of Furimsky.[2] Senol,[11] Mahfud[12] and Gutierrez et al.[13] explained the process of removing oxygen from bio-oil using HDO under high pressure in the presence of suitable catalysts such as cobalt–molybdenum or nickel–molybdenum. Mahfud[12] presented the reaction stoichiometry of the HDO process and reported that HDO is efficient in terms of carbon efficiency and saturated C=C and C=O bonds and aromatic rings while removing oxygen in the presence of H_2 and catalysts, resulting in the production of renewable liquid fuels such as gasoline and diesel. Furthermore, in extension to the earlier studies, Gutierrez et al.[14] reported that upgrading bio oil by HDO requires relatively high pressures in the range of 7–20 MPa to convert some of the compounds of bio-oils that have a low HDO reactivity to O-free products. In addition, Elliott and Hart[15] conducted semi batch HDO experiments using acetic acid and furfural to represent pyrolysis products from hemi-cellulose and cellulose, respectively, in the absence of a catalyst. The authors reported the formation of a solid polymeric material from furfural at 250 °C. Using Ru/C as the catalyst and acetic acid as the feed, they observed negligible conversions at low temperatures (<200 °C) and strong gas production at high temperatures (>250 °C). Their approach resulted in a reduction of the oxygen content from 41.3 wt% to 20–27.0 wt%.[16–18] Wildschut et al.[19] conducted HDO experiments in an autoclave using glucose and cellobiose as model compounds for the sugar fraction of pyrolysis oil. They concluded that during HDO of these model compounds using a ruthenium on carbon (Ru/C) catalyst, the catalytic hydrotreatment route is preferred over thermal decomposition, which leads to the formation of tar/solids (humins). The main products observed were polyols and gas products (mostly methane). Later Wildschut et al.[20] found that there is no formation of benzene in the product on the HDO reaction of phenol over Ru/C catalyst. Recent results of Wildschut et al.,[20] Li and Huber,[21] and de Miguel Mercader et al.[22] indicate that the HDO process removes oxygen under high pressures with a zeolite catalyst in the form of CO, CO_2 and H_2O. Furthermore, aqueous-phase reforming has been developed and tested for the bio-oil upgradation by Taarning et al.[23] Another historical review of Mortensen et al.[24] on the catalytic upgradation of bio-oil to engine fuels suggested two different paths for the upgradation process: hydrodeoxygenation and zeolite cracking. The author reported that the HDO process

mostly occurs in the temperature range of 310–350 °C and pressures of 10–140 bar. They suggested a replacement of the catalyst suitable for HDO, which includes a sulphide catalyst and a noble catalyst with a base metal catalyst; this was supported by Wang et al.[25] Moreover, HDO is found to be a suitable way to produce synthetic fuels of acceptable grade for the current infrastructure and also its usage as platform chemical to co-process in refinery units.[22,26–30] Bridgwater[7] presented a review on the fast pyrolysis of biomass and suggested that the bio refineries have the best possible scope for bio-fuel upgradation. Recently, Yaseen et al.[31] experimentally studied the HDO of fast pyrolysis bio-oils from various feedstocks using carbon-supported catalysts. They concluded that the switch grass bio-oil performed the best over Pt/C catalyst in terms of hydrogen consumption efficiency, deoxygenation efficiency, and types of bio-oil upgraded compounds. The extensive work that has been undertaken over the past 25–30 years in the field of catalytic hydrotreating of biomass-derived liquids has been thoroughly reviewed by several researchers.[32–36]

Finally, from the aforementioned extensive literature review, it can be concluded that several experimental studies on the upgradation of bio oil using HDO in the presence of suitable catalysts are available in the literature; however, analogous information on the basis of numerical studies is virtually non-existent. Therefore, this study aims to numerically investigate the performance of HDO process for the upgradation of bio oil in the presence of Pt/Al$_2$O$_3$, Ni–MO/Al$_2$O$_3$, Co–MO/Al$_2$O$_3$ catalysts over wide ranges of WHSV, temperature and pressure using a CFD approach.

Problem statement and mathematical formulation

A schematic representation of the ebullated bed reactor used in the present simulation study is shown in Fig. 1. The height of the reactor is chosen to be 0.813 m and the diameter of the reactor is chosen to be 0.01564 m. The reactor is initially packed with catalyst particles up to 0.508 m of the maximum packing limit height. The conditions for the free board and catalyst bed are specified in terms of volume fraction. The catalyst volume fractions are obtained using the following equation:

$$\in = \frac{W_s}{\rho_c A_c h} \tag{1}$$

where W_s is the weight of the solid fed to the reactor, ρ_c is the density of the catalyst, A_c is the cross section area of the reactor, h is the packing height. The volume fraction of the catalyst in the bed is calculated to be 0.0286 in the case of Pt/Al$_2$O$_3$ catalyst, and it is 0.75 for Ni–Mo/Al$_2$O$_3$ and Co–Mo/Al$_2$O$_3$ catalysts. In other words, only a volume fraction of 0.0286 (out of the initial maximum packing height of 0.508 m) is occupied by the catalyst particles when Pt/Al$_2$O$_3$ catalyst is used; similarly, a volume fraction of 0.75 is occupied by the catalyst particles when Ni–Mo/Al$_2$O$_3$ and Co–Mo/Al$_2$O$_3$ catalysts are used. The pine pyrolytic oil consisting of various lumping groups along with hydrogen (H_2) gas is introduced from the bottom of the reactor

Paper

to pass through the catalyst bed. The thermo-physical properties of three phases used in the present simulations are listed in Table 1. The oil feed rate and its velocity is calculated based on the value of the weight hourly space velocity, which is given as follows:

$$\text{WHSV} = \frac{\text{gram of pine pyrolytic oil input per hour}}{\text{gram of catalyst in reactor}} \quad (\text{h}^{-1})$$

For the gas phase inlet conditions, the minimum fluidization velocity of the gas phase is used in the present simulation studies. The bed region is initialized as a heterogeneous mixture of solid and gas phases, and the gas is fully occupied in the freeboard region.

To obtain the hydrodynamics and performance of the upgradation of bio oil, the following model equations along with appropriate reaction kinetics are solved simultaneously.

The continuity equation for all the three phases.[37]

$$\frac{\partial}{\partial t}\left(\alpha_q \rho_q\right) + \nabla \cdot \left(\alpha_q \rho_q \vec{v}_q\right) = 0 \tag{2}$$

Fluid–fluid and fluid–solid momentum equation is given by Alder and Wainwright[38]

$$\frac{\partial}{\partial t}\left(\alpha_q \rho_q \vec{v}_q\right) + \nabla \cdot \left(\alpha_q \rho_q \vec{v}_q \vec{v}_q\right) =$$
$$\alpha_q \rho_q \vec{g} + \nabla \cdot \overline{\overline{\tau_q}} - \alpha_q \nabla p + \sum_{p=1}^{n}\left(K_{pq}\left(\vec{v}_p - \vec{v}_q\right)\right) + \vec{F}_q \tag{3}$$

$$\frac{\partial}{\partial t}\left(\alpha_s \rho_s \vec{v}_s\right) + \nabla \cdot \left(\alpha_s \rho_s \vec{v}_s \vec{v}_s\right) =$$
$$\alpha_s \rho_s \vec{g} + \nabla \cdot \overline{\overline{\tau_s}} - \alpha_s \nabla p - \nabla p_s + \sum_{l=1}^{n}\left(K_{ls}\left(\vec{v}_l - \vec{v}_s\right)\right) \tag{4}$$

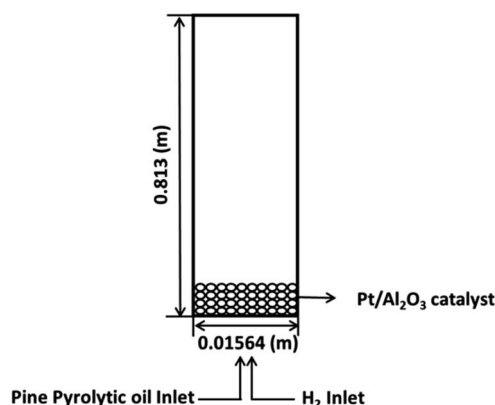Interphase momentum exchange coefficient between liquid and solid phases.[39–41]

Fig. 1 Schematic representation of the ebullated bed reactor for bio-oil upgradation using HDO.

$$K_{ls} = C_d \frac{3}{4} \rho_l \frac{\alpha_l \alpha_s}{d_s}\left|\vec{u}_s - \vec{u}_l\right|\alpha_l^{-2.65} + \frac{150\alpha_s(1 - \alpha_l)\mu_l}{\alpha_l d_s^2}$$
$$+ \frac{1.75\alpha_s \rho_l\left(\vec{u}_s - \vec{u}_l\right)}{d_s} \tag{5}$$

The drag between the solid and fluid wall is given by Schiller and Naumann[42] as

$$K_{pq} = \frac{\alpha_p \rho_p(1 + 0.15\text{Re}^{0.687})}{\tau_p} \tag{6}$$

The energy conservation equation is given as

$$\frac{\partial}{\partial t}\left(\alpha_q \rho_q h_q\right) + \nabla \cdot \left(\alpha_q \rho_q h_q \vec{u}_q\right) = -\alpha_q \frac{\partial_{pq}}{\partial t} + \overline{\overline{\tau_q}} : \nabla \vec{u}_q - \nabla \cdot \vec{q}_q + S_q$$
$$+ \sum_{p=1}^{n} \frac{\left(6c_q \alpha_q \alpha_p Nu(T_p - T_q)\right)}{d_p^2} \tag{7}$$

Fluid–fluid interaction is governed by Ranz and Marshall[43] and fluid–solid by Gunn[44]

$$Nu_p = 2.0 + 0.6\text{Re}_p^{1/2}Pr^{1/3} \tag{8}$$

$$Nu_s = (7 - 10\alpha_f + 5\alpha_f^2)(1 + 0.7\text{Re}_s^{0.2}Pr^{1/3})$$
$$+ (1.33 - 2.4\alpha_f + 1.2\alpha_f^2)\text{Re}_s^{0.7} \tag{9}$$

The turbulent kinetic energy (k) for the multiphase is governed by Launder and Spalding.[45]

$$\frac{\partial}{\partial t}(\rho k) + \frac{\partial}{\partial x_i}(\rho k u_i) = \frac{\partial}{\partial x_j}\left[\left(\mu + \frac{\mu_t}{\sigma_k}\right)\frac{\partial k}{\partial x_j}\right]$$
$$+ G_k + G_b - \rho\varepsilon - Y_M + S_k \tag{10}$$

The dissipation rate (ε) of the turbulent kinetic energy for all the phases is also explained by Launder and Spalding.[45]

$$\frac{\partial}{\partial t}(\rho\varepsilon) + \frac{\partial}{\partial x_i}(\rho\varepsilon u_i) = \frac{\partial}{\partial x_j}\left[\left(\mu + \frac{\mu_t}{\sigma_\varepsilon}\right)\frac{\partial\varepsilon}{\partial x_j}\right] + C_{1\varepsilon}(G_k + C_{3\varepsilon}G_b)$$
$$- C_{2\varepsilon\rho} - \frac{\varepsilon^2}{k} + S_\varepsilon \tag{11}$$

$$\frac{3}{2}\left[\frac{\partial}{\partial t}(\rho_s\alpha_s\theta_s) + \nabla \cdot \left(\rho_s\alpha_s\theta_s\vec{v}_s\right)\right] =$$
$$\left(-p_s\overline{\overline{I}} + \overline{\overline{T}}\right) : \nabla\vec{v}_s + \nabla \cdot (K_{\theta_s}\nabla\theta_s) - \gamma\theta_s + \varnothing_{ls} \tag{12}$$

and finally the diffusion coefficient by Ding and Gidaspow.[46]

$$K_{\theta_s} = \frac{150\rho_s d_s\sqrt{\theta\pi}}{384(1 + e_{ss})g_{0,ss}}\left[1 + \frac{6}{5}\alpha_s g_{0,ss}(1 + e_s)\right]^2$$
$$+ 2\rho_s\alpha_s^2 d_s(1 + e_{ss})g_{0,ss}\sqrt{\frac{\theta_s}{\pi}} \tag{13}$$

Table 1 Thermo-physical properties of the three phases (adopted from Stowe,[48] Raal and Muhlbauer,[49] Lin[50])

	Compound	ρ (kg m^{-3})	μ (Pa s)	C_p (J kg^{-1} K^{-1})	K (W m^{-1} K^{-1})
Pine oil	HNV	841.15	0.0009	1833.81	0.127
	LNV	679.5	0.0004	2223.19	0.140
	Phenols	1030	0.1842	1430.00	0.190
	Aromatics	880	0.0008	1699.84	0.131
	Alkane	0.669	0.00001	2222	0.033
Gas	H$_2$ (gas)	0.8189	0.000008	14 283	0.167
	Water vapour	0.5542	0.000013	2014	0.0261
Catalyst	Pt/Al$_2$O$_3$	21 450	0.000017	130	71.6
	Ni–Mo/Al$_2$O$_3$	829.75	0.000017	1360.71	0.186
	Co–Mo/Al$_2$O$_3$	829.75	0.000017	1243.47	0.2213
	Coke + ash	375	1.206	850	0.2
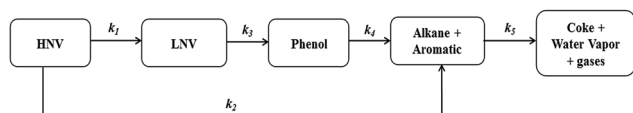
Fig. 2 Reaction pathways for the hydroprocessing of pine pyrolytic oil (Sheu *et al.*[47]).

$$r_1 = -k_1\rho_1 \tag{14}$$
$$r_2 = k_1\rho_1 - k_2\rho_2 - k_3\rho_2 \tag{15}$$
$$r_3 = k_3\rho_2 - k_4\rho_3 \tag{16}$$
$$r_4 = k_2\rho_2 + k_4\rho_3 - k_5\rho_4 \tag{17}$$
$$r_5 = k_5\rho_4 \tag{18}$$

Lumped kinetic models

Because there are many species present in both pine pyrolytic oil and its hydrotreated products, the lumping of their constituents together with similar functional groups is a useful approach for studying reaction kinetics. Moreover, the lumped kinetic models give useful insights and a clear understanding to quantify the effects of process variables on product yields. In this study, five lumping kinetic model for the hydrodeoxygenation of pyrolytic bio-oil proposed by Sheu *et al.*[47] is used, and the reaction pathway is shown in Fig. 2 and Table 2.

All these reactions are forward reactions, *i.e.*, they are irreversible and their rate equations are given as follows:

where ρ_1, ρ_2, ρ_3, and ρ_4 are the densities of the heavy non-volatiles, light non volatiles, phenols and alkane aromatics, respectively. The reaction pathways follow the forward direction alone without any backward reactions, as shown in Table 2 and Fig. 2.

Numerical methodology

The aforementioned model equations for hydrodynamics and reaction kinetics are solved simultaneously using a turbulent flow module available in the commercial CFD software ANSYS Fluent 14.5 in double precision mode. This methodology

Table 2 Lumped kinetic parameters of pine pyrolytic oil by Sheu *et al.*[47]

	HNV → LNV	HNV → alkane + aromatic	LNV → phenol	Phenol → alkane + aromatic	Alkane + aromatic → H$_2$O + gases + coke
Pt/Al$_2$O$_3$					
Activation energy, $E_a \times 10^{-7}$ (J kmol^{-1})	7.40	9.18	8.06	6.23	6.96
Arrhenius constant, A (min^{-1})	3860	75 400	8300	950	4000
Ni–Mo/Al$_2$O$_3$					
Activation energy, $E_a \times 10^{-7}$ (J kmol^{-1})	8.22	10.58	9.04	6.84	7.49
Arrhenius constant, A (min^{-1})	8800	654 000	30 600	1920	16 400
Co–Mo/Al$_2$O$_3$					
Activation energy, $E_a \times 10^{-7}$ (J kmol^{-1})	7.45	9.64	8.18	6.90	5.58
Arrhenius constant, A (min^{-1})	3500	218 000	7700	3100	450

Table 3 Validation of present results at $T = 623$ K, $P = 8720$ kPa and WHSV $= 2$ h^{-1} with the experimental results of Sheu et al.[47]

Lumped fraction	Unprocessed pyrolytic oil (wt%)[47]	Upgraded pyrolytic oil (wt%)	
		Experimental (Sheu et al.[47])	Present numerical results
HNV	0.4932	0.2457	0.2102
LNV	0.3690	0.2941	0.4083
Phenol	0.1232	0.1063	0.1552
Alkane + aromatic	0.0146	0.1952	0.1962
Coke + gas + H$_2$O	0	0.1587	0.000169

employs a finite volume approach for flow solutions, which is beneficial for the local satisfaction of the conservation equations and for relatively coarse grid modelling. As shown in Fig. 1, the velocity inlet and pressure outlet boundary conditions are used for the present simulation studies because the realistic values promote numerical convergence. For wall boundaries, no slip boundary is applied. A pressure based solver is employed to solve phasic momentum equations, shared pressure, and phasic volume fraction equations in a segregated manner. The phase coupled semi-implicit method for pressure linked equations (PC-SIMPLE) algorithm is implemented, which is an extension of the SIMPLE algorithm developed for multiphase flows. In the PC-SIMPLE method, velocities are solved coupled by phases, yet in a segregated manner. A block algebraic multigrid scheme is then used to solve a vector equation of the velocity components of all phases simultaneously. For spatial discretization, a second order upwind scheme is chosen for the momentum equation, and QUICK scheme is chosen for volume fractions. The QUICK scheme is based on a weighted average of second-order upwind and central interpolations of the variable. The time step size used for simulation is in the order of 10^{-3}. The structured quadrilateral grid is implemented using a hexahedral mesh of 12 462 nodes. The post processing of the simulation results was performed using CFD post 14.5.

Results and discussion

Validation

The results on the upgradation of bio-oil using the HDO process through numerical approach are virtually non-existent and to the best of our knowledge, only Sheu et al.[47] have reported numeric results on the upgradation of bio-oil using HDO.

Therefore, the present numerical solver is validated by comparing the present values of the mass fractions of the lumped species of the upgraded bio-oil phase with existing experimental results from Sheu et al.,[47] and this is shown in Table 3. The present results are in close proximity with the existing literature values, which gave us the confidence to proceed further to check the effects of various catalysts over a wide range of temperatures, pressures and weight hourly space velocities.
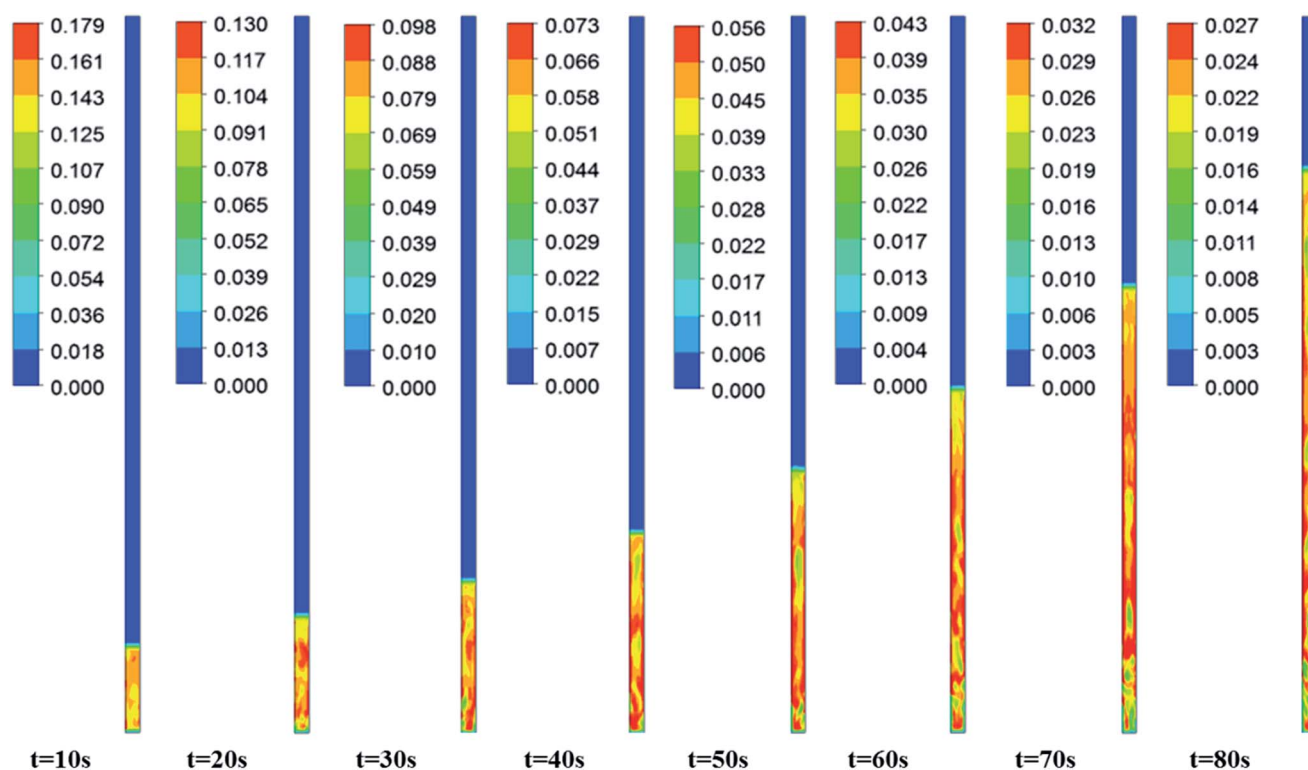

Fig. 3 Expansion of the Pt/Al$_2$O$_3$ catalyst bed at WHSV $= 3$ h^{-1}, $T = 673$ K and $P = 8720$ kPa with increasing time.

Volume fractions of upgraded pine oil, catalyst and H_2 gas

Fig. 3–5 show the prototype volume fraction images of all three phases (*i.e.*, catalyst phase in Fig. 3, pyrolytic oil phase in Fig. 4 and H_2 gas phase in Fig. 5) at $T = 673$ K and $P = 8720$ kPa at WHSV = 3 h^{-1} in the presence of Pt/Al_2O_3 catalyst. It can be noted from the volume fraction of all three phases that these phases expand with increasing time and reach a limiting maximum permissible height of 0.508 m of the bed. The volume fraction images of the catalyst phase (Fig. 3) indicate that the total volume of the catalyst remain constant though they distribute (expand) up to a bed height of 0.508 m. On the other hand, the volume fraction images of upgraded pine oil (Fig. 4) increases with increasing time, indicating the change in the composition of their lumped species and attain steady value at larger time values. The volume fraction images of H_2 gas phase (Fig. 5) indicate that most of it occupies the free board space; however, a significant amount of H_2 is also available in the bed region for the upgradation of bio-oil. Similarly, Fig. 6 denotes the steady mass fraction of the lumped species of the upgraded bio-oil obtained by the use of Pt/Al_2O_3 catalyst at WHSV = 3 h^{-1} at $T = 673$ K and $P = 8720$ kPa. The mass fraction images, shown in Fig. 6, have been obtained after the steady state has been reached, *i.e.*, the bed expansion has ceased and no further change in the composition of upgrading bio-oil is observed.

It can be seen from Fig. 6 that all the lumped species of upgraded bio-oil are expanded within the maximum limit of bed height and their composition in the free board region is zero; however, the H_2 gas escapes into the freeboard region.

Moreover, the final steady mass fractions of HNV, LNV, phenols, alkanes and aromatics in this figure are consistent with the experimental mass fractions reported by Sheu *et al.*[47] From these simulation results, it can be said that it is possible to almost completely overcome coke formation. Moreover, the water vapour (moisture) contents can be reduced to an almost negligible fraction (<2% vol) provided the experimental conditions are maintained exactly the same as in the simulations.

Fig. 7–9 show the effects of temperature, pressure and WHSV on the volume fraction of catalyst phase, H_2 gas phase and upgraded oil phase in the presence of Pt/Al_2O_3 catalyst (Fig. 7), $Ni–Mo/Al_2O_3$ catalyst (Fig. 8) and $Co–Mo/Al_2O_3$ catalyst (Fig. 9). The line legends are same for Fig. 7–9; thus, they are shown in Fig. 8 only.

In Fig. 7–9, the left y-axis depicts the corresponding volume fraction values of pine oil and the catalyst, whereas the right y-axis indicates the volume fraction values of the H_2 gas phase. It should be noted that the values of volume fraction of the three phases presented in Fig. 7–9 are steady state values, *i.e.*, obtained after the bed has attained steady state by expanding up to the maximum attainable bed height. These volume fraction values also indicate that there is no further change in their values with increasing time. Fig. 7 shows the variations in the volume fraction of upgraded oil, H_2 gas and Pt/Al_2O_3 catalyst for different values of WHSV, temperature and pressure. The pine oil volume fraction shows a mixed trend with respect to temperature and pressure at WHSV = 2 h^{-1} (Fig. 7a); however, at WHSV = 3 h^{-1} (Fig. 7b) and WHSV = 4 h^{-1} (Fig. 7c), it increases with increase in the temperature to $T = 673$ K.
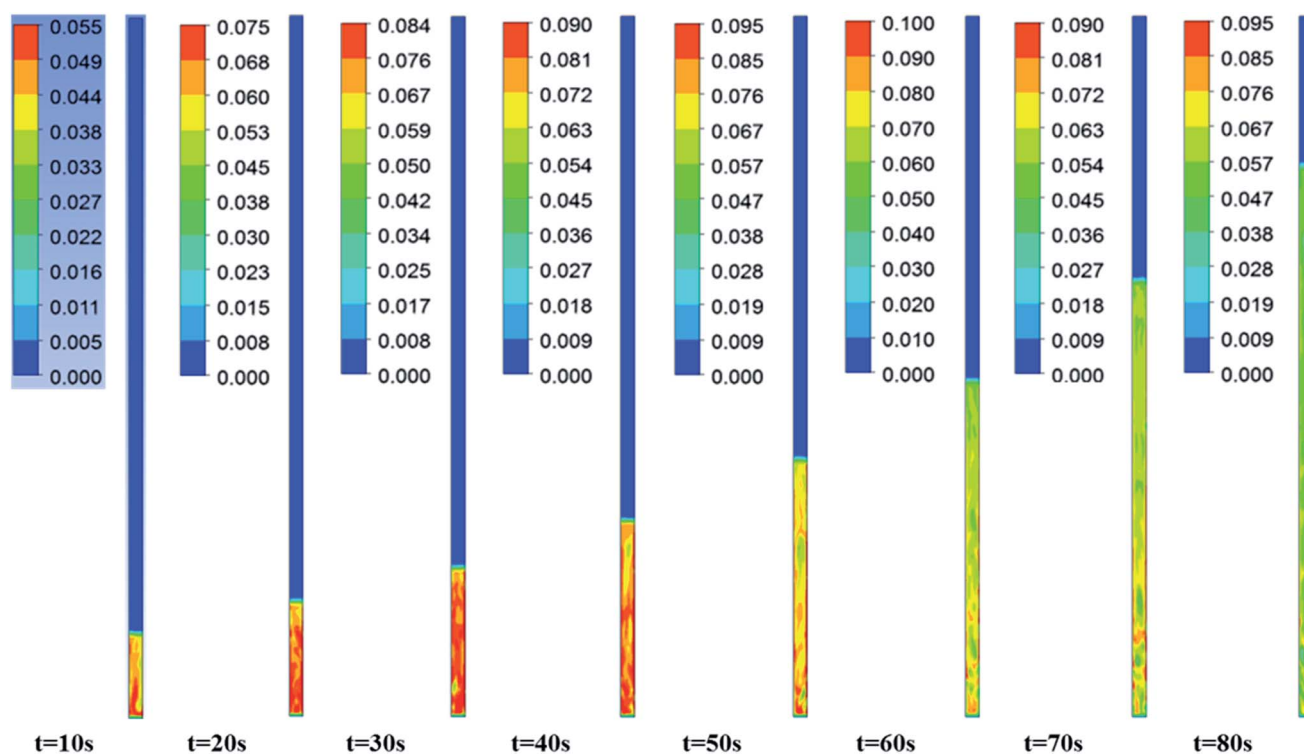

Fig. 4 Volume fraction images of the pine pyrolytic oil phase with increasing time at WHSV = 3 h^{-1}, $T = 673$ K and 8720 kPa in the presence of Pt/Al_2O_3 catalyst.
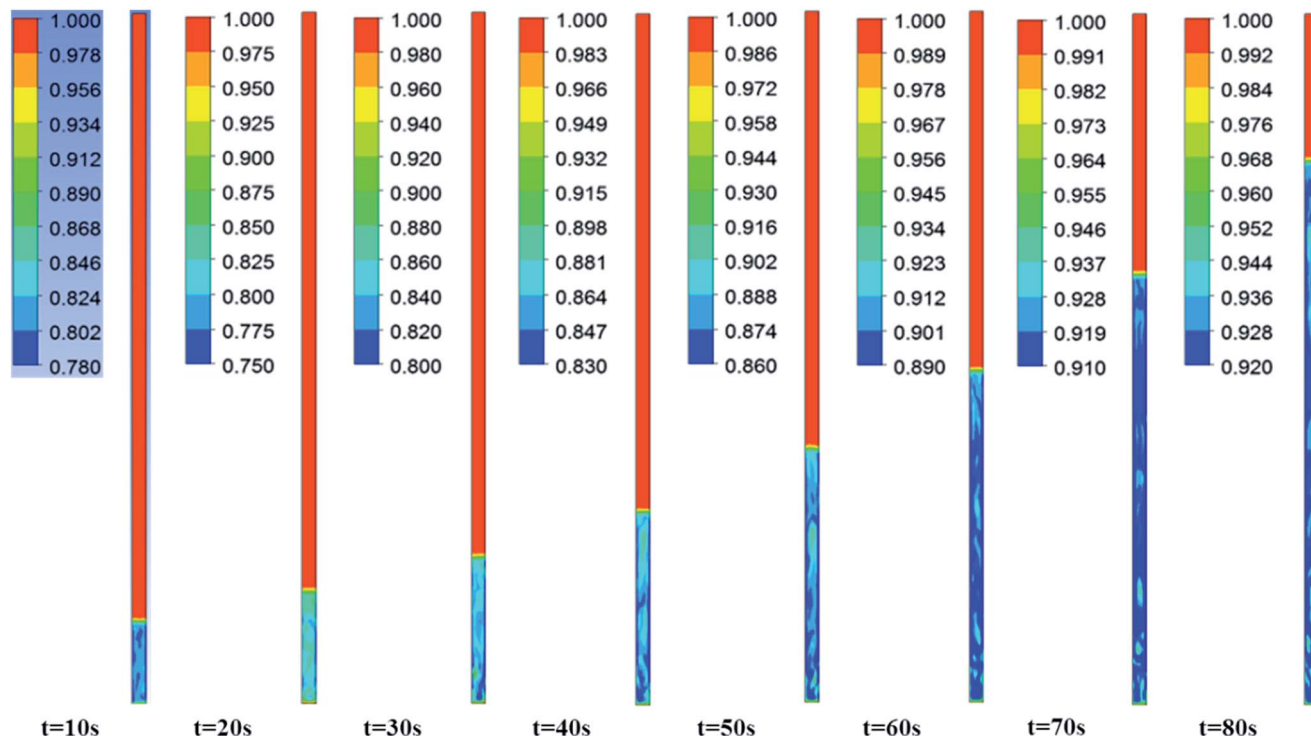
Fig. 5 Volume fraction of the H_2 gas phase with increasing time at WHSV = 3 h^{-1}, T = 673 K and 8720 kPa in the presence of Pt/Al$_2$O$_3$ catalyst.
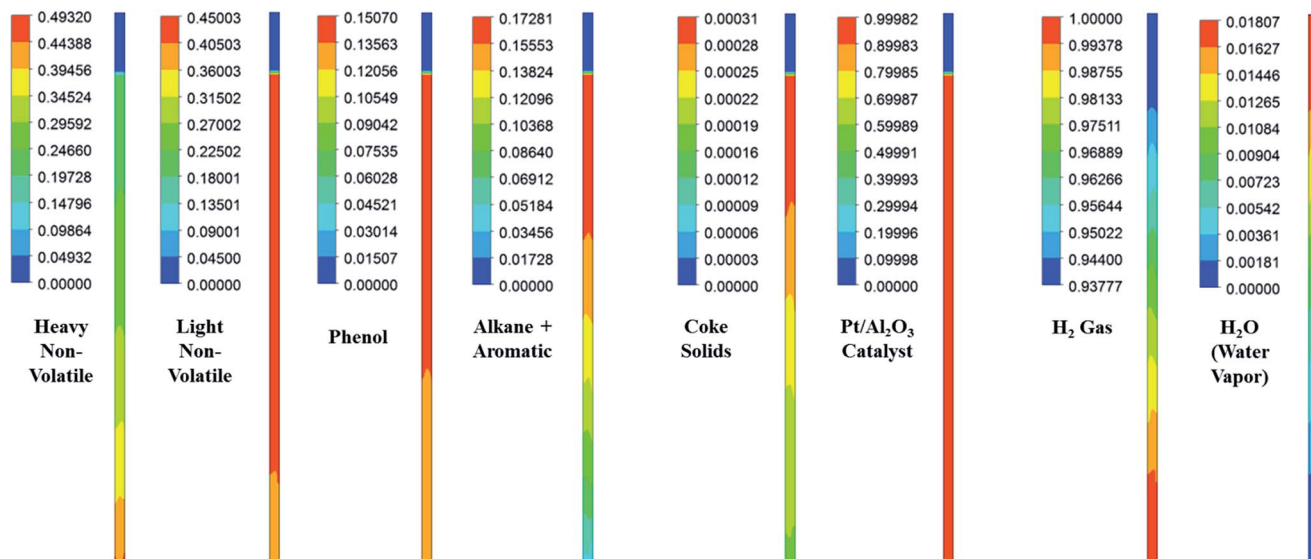

Fig. 6 Steady mass fraction images of the lumped species of upgraded pyrolytic oil and those of solid and gas/vapour phases in the presence of Pt/Al$_2$O$_3$ catalyst at WHSV = 3 h^{-1}, T = 673 K and P = 8720 kPa.

However, at a fixed temperature, the volume fraction of pine oil is almost unaffected by WHSV and pressure.

In the case of Ni–Mo/Al$_2$O$_3$ catalyst, the variation in catalyst expansion behaviour is almost negligible with the change in WHSV, temperature and pressure (Fig. 8). For the WHSV value of 2 h^{-1} (Fig. 8a), the steady volume fraction of H_2 gas slightly decreases with pressure at T = 623 K, whereas at other temperatures, the volume fraction of H_2 gas shows a mixed

trend with increasing pressure. On increasing the WHSV value to 3 h^{-1} (Fig. 8b), the volume fraction of H_2 gas at P = 6996 kPa is unaffected by the temperature; however, as the pressure increases to P = 8720 and 10 444 kPa, mixed variations in the volume fraction of H_2 gas are seen with increasing temperature. On further increasing the WHSV to 4 h^{-1} (Fig. 8c), the volume fraction of H_2 gas at a given temperature and pressure increased in comparison to the case of WHSV = 3 h^{-1} (Fig. 8b). However,

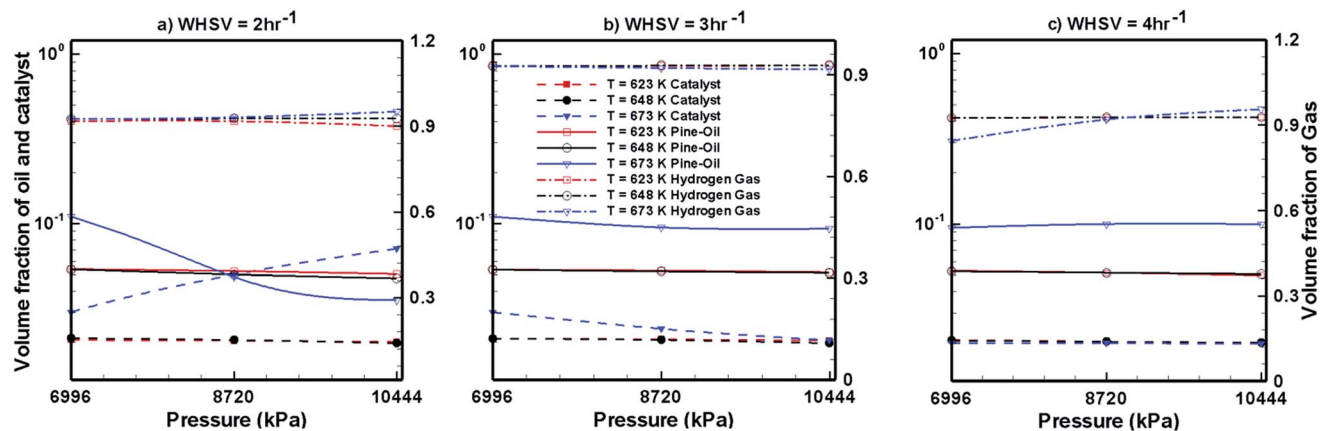**Fig. 7** Steady volume fractions of pine oil, H_2 gas and Pt/Al_2O_3 catalyst at different temperatures and pressures.

the volume fraction of H_2 gas shows mixed variations with respect to temperature and pressure in the case of WHSV = 4 h^{-1}. In the case of pine oil, the variations in their volume fraction with respect to temperature, pressure and WHSV values are very small and mixed behaviour is observed against changes in the operating conditions.

Fig. 9 shows the volume fraction of upgraded bio-oil, H_2 gas and Co–Mo/Al_2O_3 catalyst for different WHSV, temperature and pressure values. The expansion of the catalyst bed is almost unaffected by WHSV, temperature and pressure. The volume fraction of H_2 gas slightly increases with increasing pressure and temperature; however, mixed trends of H_2 gas are seen with respect to the WHSV values. The volume fraction of pine oil decreases with increasing pressure and temperature; however, it increases with increasing WHSV values when Co–Mo/Al_2O_3 catalyst is used. Finally, by comparing the performance of all the catalysts (Fig. 7–9), it can be seen that Pt/Al_2O_3 produces a larger fraction of upgraded pine oil, whereas Ni–Mo/Al_2O_3 produces a smaller volume fraction of the upgraded bio-oil.

Mass fraction of lumped species of upgraded bio oil

Fig. 10 and 11 show the steady mass fraction values of the lumped species of upgraded bio-oil by HDO process in the

presence of Pt/Al_2O_3 catalyst for the different combinations of WHSV, temperature and pressure. The mass fraction values reported in these figures are obtained when the bed has reached pseudo steady state. Fig. 10 shows the steady mass fractions of lumped HNV and LNV in the presence of Pt/Al_2O_3 catalyst. At WHSV = 2 h^{-1}, the steady mass fraction of LNV decreases slightly with increasing pressure and decreasing temperature. At WHSV = 3 h^{-1}, the variation in the mass fraction of LNV is negligible with changes in temperature and pressure. At WHSV = 4 h^{-1}, mixed variations in the steady state mass fractions of LNV are observed with respect to temperature and pressure. The mass fractions of HNV at WHSV = 2 h^{-1} (Fig. 10a) and WHSV = 4 h^{-1} (Fig. 10c) show a mixed trend with respect to temperature and pressure; however, at WHSV = 3 h^{-1} (Fig. 10b), at a given temperature, the mass fraction of HNV slightly decreases with increasing pressure. The variation in the mass fraction of HNV at WHSV = 3 h^{-1} (Fig. 10b) and a fixed value of pressure shows a mixed trend with respect to temperature. From Fig. 11a, it can be seen that the mass fractions of phenols, alkanes and aromatics show a mixed trend with respect to the WHSV, temperature and pressure.

Fig. 12 shows the variations in mass fraction values of lumped HNV and LNV species in the upgraded bio-oil by the HDO
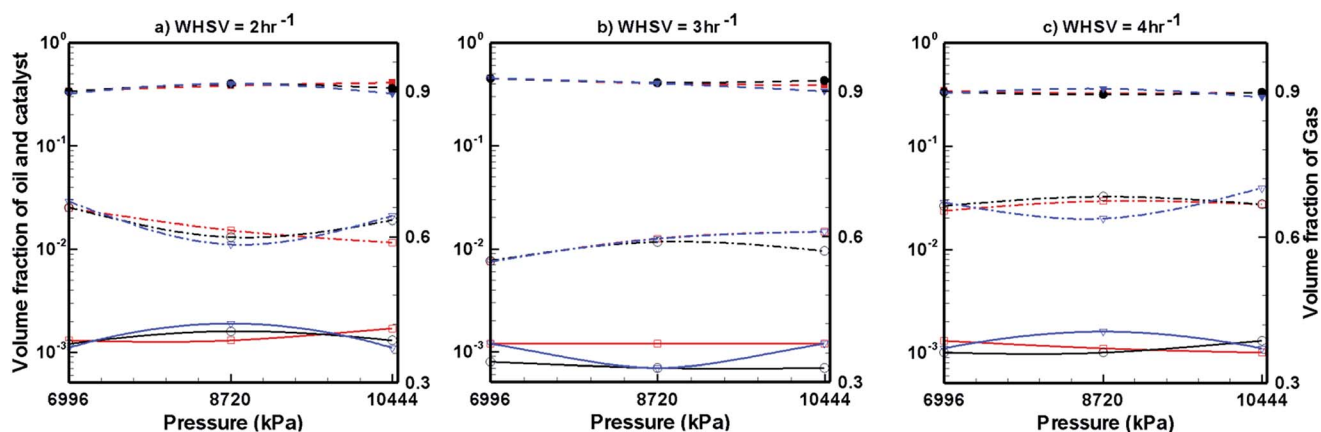

Fig. 8 Steady volume fractions of pine oil, H_2 gas and Ni–Mo/Al_2O_3 catalyst at different temperatures and pressures.
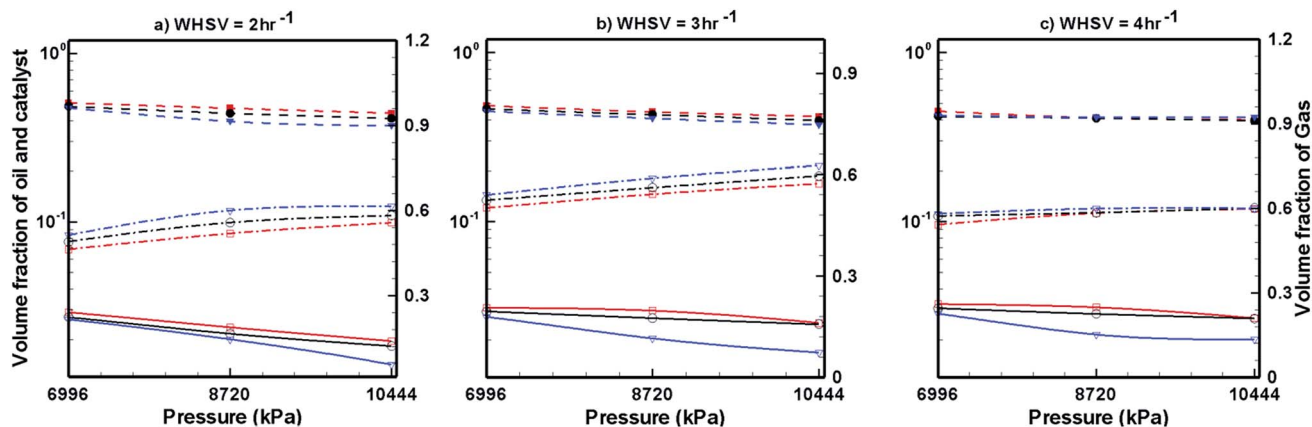
Fig. 9 Steady volume fractions of pine oil, H_2 gas and Co–Mo/Al_2O_3 catalyst at different temperatures and pressures.
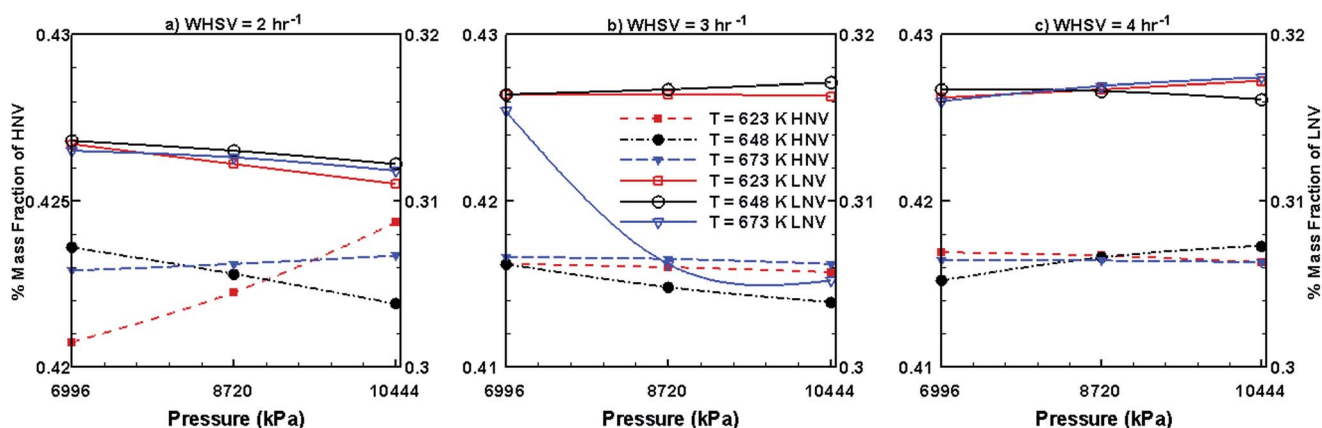

Fig. 10 Mass fractions of HNV and LNV obtained by upgrading pine oil in the presence of Pt/Al_2O_3.

process in the presence of Ni–Mo/Al_2O_3 catalyst, and the mixed trends can be seen here too with respect to WHSV, temperature and pressure. However, compared to the Pt/Al_2O_3 catalyst, (Fig. 10) the mass fractions of HNV and LNV obtained by the use of Ni–Mo/Al_2O_3 has substantially decreased for fixed combinations of WHSV, temperature and pressure.

Fig. 13 shows the variations in the steady mass fractions of lumped phenols, alkanes and aromatics obtained by the HDO of bio-oil in the presence of Ni–Mo/Al_2O_3, and mixed trends are seen for changes in WHSV, temperature and pressure. However, compared to Pt/Al_2O_3 (Fig. 11), Ni–Mo/Al_2O_3 catalyst (Fig. 13)
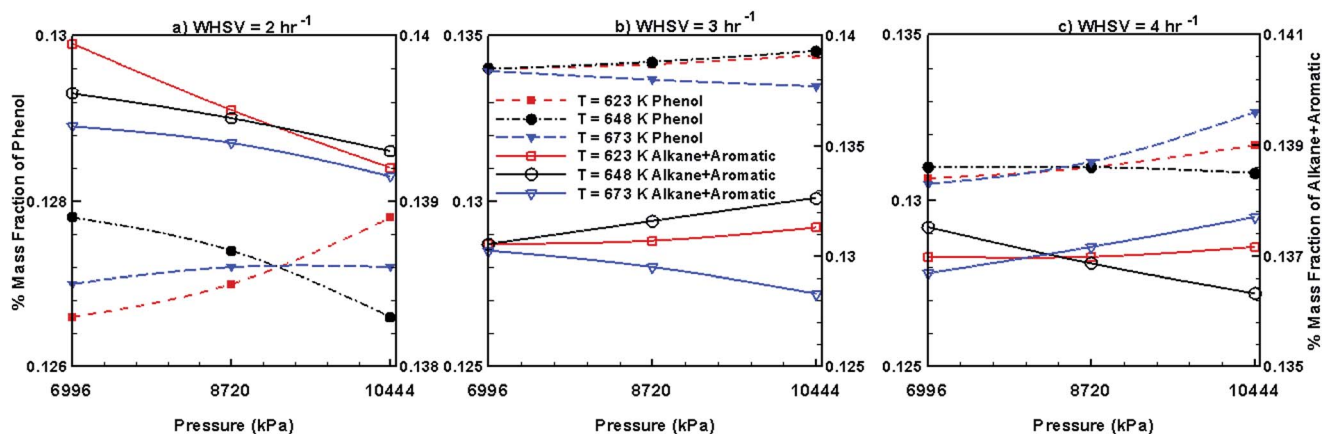

Fig. 11 Mass fractions of phenols, alkanes and aromatics obtained by upgrading pine oil in the presence of Pt/Al_2O_3.
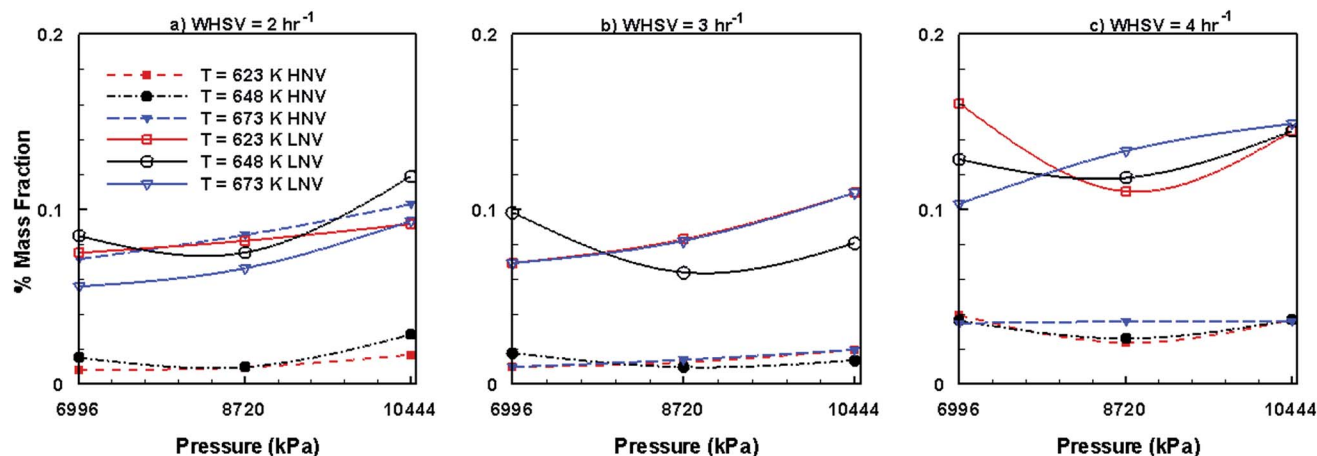
Fig. 12 Mass fractions of HNV and LNV obtained by upgrading pine oil in the presence of $Ni-Mo/Al_2O_3$.
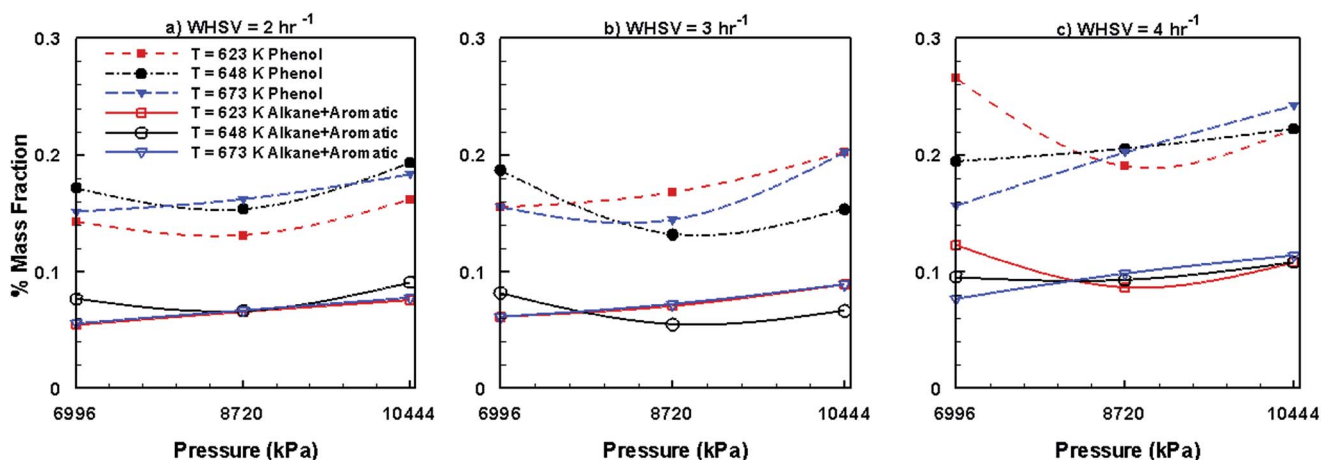

Fig. 13 Mass fractions of phenols, alkanes and aromatics obtained by upgrading pine oil in the presence of $Ni-Mo/Al_2O_3$.

produces larger mass fractions of phenols but smaller fractions of alkanes and aromatics.

Fig. 14 shows the mass fractions of HNV and LNV obtained by the use of $Co-Mo/Al_2O_3$ catalyst. It can be seen from this figure that the mass fractions of both HNV and LNV decrease with increasing pressure, temperature and WHSV. In comparison to other catalysts, $Ni-Mo/Al_2O_3$ produces small fractions of HNV and LNV followed by Pt/Al_2O_3 catalyst and $Co-Mo/Al_2O_3$
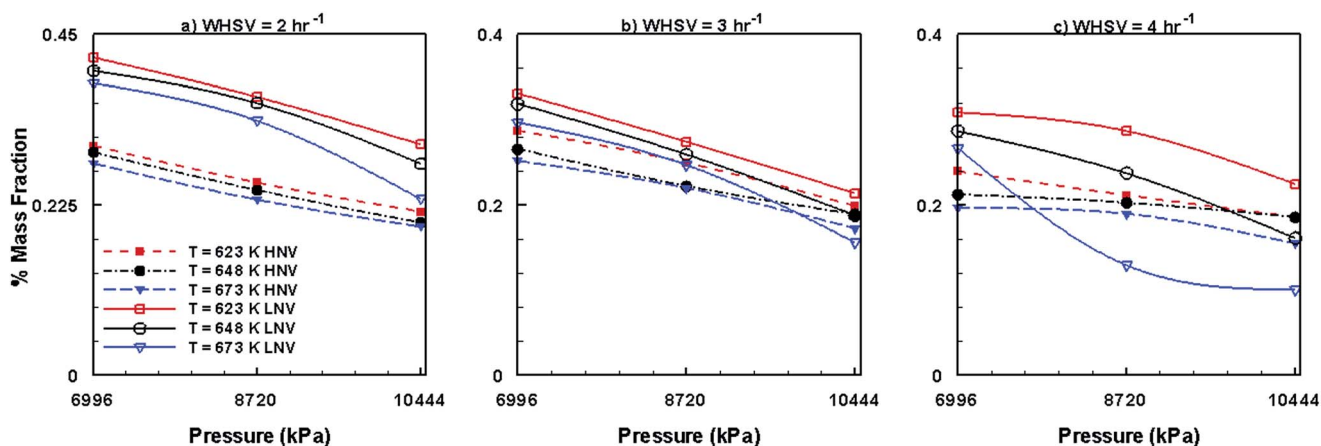

Fig. 14 Mass fractions of HNV and LNV obtained by upgrading pine oil in the presence of $Co-Mo/Al_2O_3$.
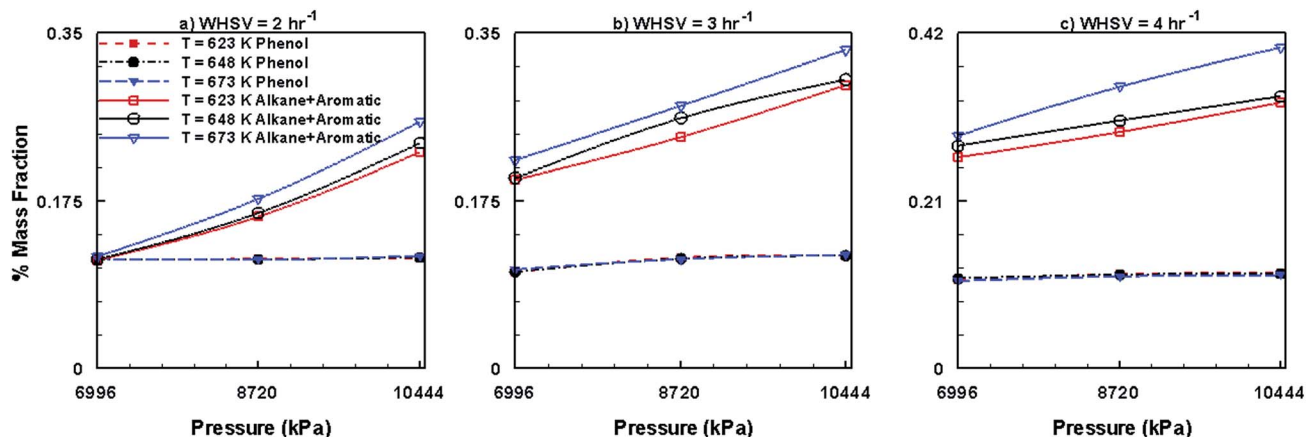
Fig. 15 Mass fractions of phenols, alkanes and aromatics obtained by upgrading pine oil in the presence of Co–Mo/Al$_2$O$_3$.

catalyst producing larger fractions of HNV and LNV. Fig. 15 presents the mass fractions of phenols, alkanes and aromatics obtained by the use of Co–Mo/Al$_2$O$_3$ catalyst. It can be seen from Fig. 15 that the formation of phenols by the use of Co–Mo/Al$_2$O$_3$ is almost unaffected by temperature, pressure and WHSV values; however, the fractions of alkanes and aromatics increase with increasing pressure, temperature and WHSV. On comparing with other two catalysts, Co–Mo/Al$_2$O$_3$ catalyst produces larger fractions of alkanes and aromatics followed by Pt/Al$_2$O$_3$ and Ni–Mo/Al$_2$O$_3$, producing smaller fractions of alkanes and aromatics.

Conclusions

This numerical work presents the advancement of suitable catalysts for the upgradation of bio-oil through a HDO process in an ebullated bed reactor at temperatures running between 623 K $\leq T \leq$ 673 K, pressure ranges between 6996 kPa $\leq P \leq$ 10 443 kPa and WHSVs varying between 2 $\leq$ WHSV (h^{-1}) $\leq$ 4. The consequences of this study demonstrate some important and significant behaviour of the three phases under the influence of three different catalysts, namely, alumina supported platinum, Co–Mo, and Ni–Mo catalysts. Some of the key findings of this study include the fact that the gas volume fraction is higher in the case of Pt/Al$_2$O$_3$ catalyst. The amount of phenol formation during the upgradation process is significant and effective in the case of Ni–Mo/Al$_2$O$_3$ catalyst compared to the other catalysts. The amount of aromatic formation is larger by the use of Co–Mo/Al$_2$O$_3$ catalyst in comparison with the other catalysts. The higher values of the volume and the mass fractions of upgraded lumped species are obtained at low WHSV values and high temperatures and pressures.

Acknowledgements

References

1 A. Oasmaa, D. Meier and A. Bridgwater, *Fast Pyrolysis of Biomass: A Handbook*, CPL Press, Newbury, UK, 2002, vol. 1.
2 E. Furimsky, *Appl. Catal., A*, 2000, **199**, 147.
3 J. D. Adjaye and N. N. Bakhshi, *Biomass Bioenergy*, 1995, **8**, 265–277.
4 K. L. Hew, A. M. Tamidi, S. Yusup, K. T. Lee and M. M. Ahmad, *Bioresour. Technol.*, 2010, **101**, 8855–8858.
5 Z. Tang, L. Qiang, Z. Ying and G. Qingxiang, *Ind. Eng. Chem. Res.*, 2009, **48**, 6923–6929.
6 Y. Zhang, W. Li, S. Zhang, Q. Xu and Y. Yan, *Chem. Eng. Technol.*, 2012, **35**, 302–308.
7 A. V. Bridgwater, *Biomass Bioenergy*, 2012, **38**, 68–94.
8 E. Furimsky, *Catal. Rev.: Sci. Eng.*, 1983, **25**, 421.
9 S. T. Oyama, *The Chemistry of Transition Metal Carbides and Nitrides*, Blackie Academic and Professional, Springer, Glasgow, 1996.
10 R. Maggi and B. Delmon, *Stud. Surf. Sci. Catal.*, 1997, **106**, 99.
11 O. Senol, PhD thesis, Helsinki University of Technology, 2007.
12 F. H. Mahfud, PhD thesis, University of Gronigen, 2007.
13 A. Gutierrez, M. E. Domine and Y. Solantausta, Co-processing of upgraded bio-liquids in standard refinery units-fundamentals, *15th European Biomass Conference and Exhibition*, Berlin, 7–11 May 2007.
14 A. Gutierrez, R. K. Kaila, M. L. Honkela and R. Siloor, *Catal. Today*, 2009, **147**, 239–246.
15 D. C. Elliott and T. R. Hart, *Energy Fuels*, 2009, **23**, 631–637.
16 D. C. Elliott and E. G. Baker, Process of Upgrading Biomass Pyrolyzates, *US Pat.*, 4795851, 1989.
17 D. C. Elliott, *Energy Fuels*, 2007, **21**, 1792–1815.
18 D. C. Elliott, G. G. Neuenschwander and T. R. Hart, *ACS Sustainable Chem. Eng.*, 2013, **1**, 389–392.
19 J. Wildschut, I. M. Cabrere and H. J. Heeres, *Ind. Eng. Chem. Res.*, 2009, **48**, 10324–10334.
20 J. Wildschut, M. Iqbal, F. H. Mahfud, I. Melian Cabrera, R. H. Venderborsch and H. J. Herres, *Energy Environ. Sci.*, 2010, **3**, 962–970.
21 N. Li and G. W. Huber, *J. Catal.*, 2010, **270**, 48–59.

22 F. de Miguel Mercader, M. J. Groeneveld, S. R. A. Kersten, N. W. J. Way, C. J. Schaverien and J. A. Hogendoorn, *Appl. Catal., B*, 2010, **96**, 57–66.

23 E. Taarning, C. M. Osmundsen, X. Yang, B. Voss, S. I. Andersen and C. H. Chritensen, *Energy Environ. Sci.*, 2011, **4**, 793–804.

24 P. M. Mortensen, J. D. Grunwaldt, P. A. Jensen, K. G. Knudsen and A. D. Jensen, *Appl. Catal., A*, 2011, **407**, 1–19.

25 Y. Wang, Y. Fang, T. He, H. Hu and J. Wu, *Catal. Commun.*, 2011, **12**, 1201–1225.

26 W. Baldauf, U. Balfanz and M. Rupp, *Biomass Bioenergy*, 1994, **7**, 237–244.

27 G. Fogassy, N. Thegarid, Y. Schuurman and C. Mirodatos, *Green Chem.*, 2012, **14**, 1367–1371.

28 E. G. Baker and D. C. Elliott, Method of Upgrading Oils Containing Hydroxyaromatic Hydrocarbon Compounds to Highly Aromatic Gasoline, *US Pat.*, 5180868, 1993.

29 T. Choudhary and C. Phillips, *Appl. Catal., A*, 2011, **397**, 1–12.

30 R. H. Venderbosch, A. R. Ardiyanti, J. Wildschut, A. Oasmaa and H. J. Heeres, *J. Chem. Technol. Biotechnol.*, 2010, **85**, 674–686.

31 E. Yaseen, C. A. Mullen, A. L. M. T. Pighinelli and A. A. Boateng, *Fuel Process. Technol.*, 2014, **123**, 11–18.

32 J. P. Diebold and J. W. Scahill, *Energy Prog.*, 1988, **8**, 59–65.

33 E. M. Ryymin, M. L. Honkela, T. R. Viljava and A. O. I. Krause, *Appl. Catal., A*, 2010, **389**, 114–121.

34 C. Zhao, S. Kasakov, J. He and J. A. Lercher, *J. Catal.*, 2012, **296**, 12–23.

35 H. Y. Zhao, D. Li, P. Bui and S. T. Oyama, *Appl. Catal., A*, 2011, **391**, 305–310.

36 Y. Zhao, L. Deng, B. Liao, Y. Fu and Q. Xiang Guo, *Energy Fuels*, 2010, **24**, 5735–5740.

37 FLUENT Inc., *FLUENT User's Guide*, 2006.

38 J. Alder and T. E. Wainwright, *J. Chem. Phys.*, 1960, **33**, 1439–1451.

39 D. Gidaspow, R. Bezburuah and J. Ding, *Proceedings of the seventh Engineering Foundation Conference on Fluidization*, Australia, 1992.

40 C. Y. Chen and Y. H. Hu, *Chem. Eng. Prog., Symp. Ser.*, 1966, **62**, 100–111.

41 S. Ergun, *Chem. Eng. Prog.*, 1952, **48**, 89–94.

42 L. Schiller and Z. Naumann, *Z. Ver. Dtsch. Ing.*, 1933, **77**, 318–320.

43 W. E. Ranz and W. R. Marshall, *Chem. Eng. Prog.*, 1952, **48**, 141–146.

44 D. J. Gunn, *Int. J. Heat Mass Transfer*, 1978, **21**, 467–478.

45 B. E. Launder and D. B. Spalding, *Lectures in mathematical models of turbulence*, Academic Press, London and New York, 1972.

46 J. Ding and D. Gidaspow, *AIChE J.*, 1990, **36**, 523–528.

47 Y. H. E. Sheu, R. G. Anthony and E. J. Soltes, *Fuel Process. Technol.*, 1988, **19**, 31–50.

48 L. R. Stowe, Method of Conversion of Heavy Hydrocarbon Feedstocks, *US Pat.*, 5547563, 1996.

49 D. J. Raal and A. Muhlbauer, *Phase Equilibria: Measurement and Computation*, Taylor and Francis, Washington, USA, 1997.

50 S. C. Lin, Hydrocarbons via catalytic hydrogen treatment of wood pyrolytic oil, PhD thesis, A&M University, Texas, 1981.